

Pathways into the Pacific Equatorial Undercurrent: A Trajectory Analysis

Paul J. Goodman

Wilco Hazeleger

Pedro de Vries

Mark Cane

In press:

Journal of Physical Oceanography

7 June 2005

Abstract

A time-dependent trajectory algorithm is used to determine the sources of the Pacific Equatorial Undercurrent (EUC) in a global climate model with 1/4 degree (eddy-permitting) resolution and forced with realistic winds. The primary sources and pathways are identified and the transformation of properties in temperature/salinity space are explored. An estimate for the quantity of recirculation, a notoriously difficult property to estimate from observational data, is given. Over two-thirds of the water in the Pacific EUC at 140°W originates south of the equator. 70% of the EUC is ventilated outside of the tropics (poleward of 13°S or 10°N): three quarters of these extratropical trajectories travel through the western boundary currents between their subduction and incorporation into the EUC and one fifth of the extratropical trajectories enter and leave the tropical band at least once before entering the EUC.

1. Introduction

The Equatorial Undercurrent (EUC) in the Pacific Ocean lies at the base of the equatorial thermocline and is the source of the water that upwells into the thermocline. The EUC was rediscovered by Cromwell, et al. (1954), and has been mapped over the years by several studies, most notably the Tahiti-Hawaii Shuttle Experiment (Wyrtki and Kilonsky, 1984), and as part of the World Ocean Circulation Experiment (WOCE). The relative contributions from the various sources of the EUC determine the temperature, salinity, and nutrient properties of the equatorial thermocline and will affect biological productivity, carbon exchange with the atmosphere, and the ENSO cycle. Studies based on chlorofluorocarbon, tritium, silicate, and nutrient data [Tsuchiya, 1981, Tsuchiya, 1989, Fine, et al., 1994, Fine, et al., 2001] have shown that the water in the EUC comes primarily from the South Pacific, but due to the complicated current structure in the Western Equatorial Pacific, the locations where the temperature and salinity properties of the EUC are set remain elusive. Fine, et al. (1994) discuss the importance of the Western Equatorial Pacific as a water mass crossroads and attribute many of the properties there to the low-latitude western boundary currents that flow equatorward along the eastern coasts of Australia, New Zealand, and the Philippines.

Johnson and McPhaden (1999), on the other hand, find that there is a significant contribution from direct interior pathways within the subtropical pycnocline.

The Equatorial Undercurrent has also been linked to longer-term (decadal) climate variability. Gu and Philander (1997) propose that extratropical sea surface temperature anomalies are communicated to the tropics via the inter-gyre exchange, reappearing along the equator several years after being incorporated into the EUC and brought back to the surface. Zhang, et al. (1998) cite a subsurface ocean "bridge" to explain the relationship between the warm sea surface temperature (SST) anomaly in the North Pacific during the early 1970's and the subsequent warm SST anomaly along the equator in the 1980's. Schneider, et al. (1999) and Hazeleger, et al. (2001b), however, have shown that the equatorial warming was more likely caused by changes in the low-latitude wind stress.

We are going to test two competing theories about the sources of EUC water: either tropical recirculation between the undercurrent and the surrounding water sets the EUC's properties; or, the EUC's properties are determined through inter-gyre exchanges that communicate extratropical forcing to the equatorial region. We chose to do this analysis on the results from the Ocean Circulation and Climate Advanced Modeling Project (OCCAM). This simulation is global in scope, has an eddy-permitting resolution, and uses realistic winds for an improved simulation of inter-gyre transfer. Previous studies have used trajectory analysis to look at various aspects of the Pacific EUC. Lu, et al. (1998) used a 3 and 1/2 layer model of the Pacific to study the tropical cells and to give a quantitative estimate of the sources of the EUC water. Blanke and Raynaud (1997) use a slightly coarser resolution OGCM simulation of the world from 65°S to 47°N, forced with the Hellerman and Rosenstein wind climatology to quantify the local exchanges as the EUC flows from Indonesia to Peru. Huang and Liu (1999) examined the tropical-subtropical exchange using the Florida State University (FSU) wind climatology, but in a Pacific-only model with no Indonesian Throughflow.

We use the mean seasonal averages of the more detailed OCCAM output to derive our mean ocean state, and we choose to ignore variability. The seasonal mean is adequate to resolve processes that take many years and sensitivity experiments we conduct using five-day averages are not significantly different.

This study is a hydrographic analysis of the sources of the EUC and the transformation of its constituent water masses. The output from a model simulation is explored by backtracking trajectories along streamlines until they reach the mixed layer. Rodgers, et al. (2003) carried out a similar study exploring extratropical sources of the EUC in the Ocean Parallelise (OPA) model, although they employed a different trajectory algorithm as well as different starting and ending criteria. Differences between that study and the other earlier studies and this one will be noted as they arise. Temperature and salinity properties are mapped onto the trajectories to give an indication of where these properties are changed. We perform quantitative calculations of the transports from various locations and from various initial water masses as they are transformed into the relatively uniform core of the EUC.

We first discuss the data, algorithms, and procedures used in this study. We then discuss the effects of seasonality, residual mean versus Eulerian mean velocity fields, particle size, and seeding frequency related to the statistics provided by the trajectory algorithm. We next describe the sources of the EUC based on both their location and their water mass characteristics. This is followed by a hydrographic analysis of the transformations experienced along the various trajectories and a brief discussion of the implications.

2. Data and Procedures

2.1 The OCCAM Model

This study uses model output obtained from calculations with the Ocean Circulation and Climate Advanced Modeling Project (OCCAM, Webb, et al., 1997; Saunders, et al., 1999) simulation as the source of data to which the trajectory algorithm is applied. The OCCAM simulation is discussed fully in Webb, et al. (1998), and only the relevant details will be discussed here. The data is on a $0.25^\circ \times 0.25^\circ$ grid with 36 levels spanning 5500m, increasing from 20m at the surface to 255m at the bottom, covering the entire globe. The model's surface temperature and salinity were restored to the surface temperature and salinity fields from the World Ocean Atlas (Levitus and Boyer, 1994; Levitus, et al., 1994, WOA94 hereafter) with a time scale of 30 days. The

monthly-averaged wind stresses from European Center for Medium-range Weather Forecasts (ECMWF calculated from years 1986-1988, Gibson, et al., 1997) are applied for the first 8 years of the simulation. In the following three years, the six-hourly winds and wind stresses for 1993-1995 are applied. A Laplacian scheme for horizontal diffusion and viscosity is used with coefficients of $100 \text{ m}^2/\text{s}$ and $200 \text{ m}^2/\text{s}$, respectively. The vertical mixing of tracers is according to the Richardson number dependent scheme by Pacanowski and Philander (1981) that results in vertical diffusivities of $0.5 \text{ cm}^2/\text{s}$ away from regions with strong shear.

The OCCAM simulation spanned 11 years; data from years 9-11 inclusive were averaged seasonally and annually to create the various datasets. It must be noted that 11 years is not a very long simulation and there is still drift in the deeper water column. Lee, et al. (2002) have shown that drift is significant only for deeper water masses, which are not considered in this paper. We are focused on the surface and upper thermocline, however, which respond primarily to the wind forcing and should be well established after this time. The OCCAM run was initialized from WOA94, so the mixing processes that are driven by subduction are, to first order, included in the simulation. Moreover, overturning streamfunctions in density coordinates show that below the mixed layer and at depths above about 500 m ($\sim\sigma_\theta = 26.8$) the diapycnal transports are small in the model (see Fig. 1d of Hazeleger, et al., 2001 and Fig. 5d of Hazeleger, et al., 2003). We, therefore, feel confident that our results are robust.

Transports obtained from mean velocities will be referred to as the Eulerian mean transports. These do not completely describe the advection of water masses, as the latter generally follow isopycnal surfaces that may move as a function of time. The eddy/variability-induced or "residual" transports arise due to the correlation between layer thickness and velocity variations (McDougall, 1998, McIntosh and McDougall, 1996, Drijfhout, et al, 2003). These residual transports, which are calculated from the 5-day running mean data, need to be taken into account or else spurious diapycnal forces may be introduced into the calculations. The simulated velocities and layer thicknesses were correlated and time-averaged over years and seasons. We add these residual transports to the Eulerian mean transports to obtain fields which will be referred to as

Residual mean transports (Hazeleger, et al., 2001a, Hazeleger, et al., 2003). Note that interannual variabilities also give rise to residual transports.

2.2 The Trajectory Algorithm

The time-dependent trajectory algorithm employed in this study was developed by de Vries and Döös (2001) and is a descendant of the steady-state trajectory algorithm developed by Döös (1995) and Blanke and Raynaud (1997). The trajectory algorithm allows for time-varying velocity data to be incorporated into the trajectory analysis. The effect of neglecting this time interpolation has been studied in Drijfhout, et al (2003). Because season-to-season data variations are much larger than month-to-month ones, sudden switches of season introduce large, spurious diapycnal transports. Errors of up to 20% were found if no interpolation was used. To retain a correct mean seasonal cycle all seasonally-varying fields were interpolated according to the method of Killworth (1996). Each particle is volume conserving and follows true streamlines through the simulated velocity field. The method used here follows mass, not tracers. Therefore: 1) it is essential that it is volume conserving; 2) a trajectory is assigned a specific transport; and, 3) its value should be small enough to resolve divergences and convergences of streamlines; in other words, in regions of high velocity shear, numerics may create inconsistent statistics of trajectories through these regions when the particle size is too large. The other quantities, like temperature and salinity are followed along-trajectory, that is, these are given by the model which does include diffusion. The streamlines themselves also implicitly contain the effects of momentum diffusion.

Since the trajectory model only requires the velocity fields, which are known for each season, it can trace the particles forward or backward in time. Note that we are following transports and streamlines, not tracers: trajectory ages will not necessarily equal tracer ages. Trajectories represent tracers only in a "center-of-mass" fashion, and the "trajectory age" is precisely the advective age. In this study we will only refer to the *median* age when giving statistics of transit times for the trajectories. The use of a *mean* age weights those trajectories that take the longest.

The particles are seeded uniformly in space over the face of each grid-box that meets the starting criteria (Blanke and Raynaud, 1997). The number of particles is

proportional to the transport across the face of the grid-box. In this way they are grouped in regions where the transport is highest. Each particle's trajectory is then individually calculated from one grid-box to the next until it reaches the ending criteria. The trajectory algorithm keeps track of the time elapsed and the position and direction of the particle. It has also been configured to interpolate the temperature, salinity and density of the local environment (as simulated by OCCAM) onto the position of the particle at several intermediary sections between its starting and ending locations. At each intermediary crossing (of a predetermined latitude or longitude), we recorded the location, temperature, salinity, density, and age of the last crossing before entering the EUC, as well as the volume of total crossings for each trajectory in order to get some idea of the recirculations present in the model. Since the particles themselves do not change their volume, the total number of crossings at a given section can be determined by the adding the volume of the particle to the total each time it crosses.

In the seasonal runs, we performed several experiments in which the seeding frequency was varied. In the first case the particles are seeded at the middle of each season; in the next case, we seeded the same number of particles at 4 different times during each season (16 seedings over the course of the year), and in the last case we seeded eight times per seasons (32 total seedings). The diagnosed trajectories, transports, and water mass transformations were quite robust to the seeding frequency in that each run differed by no more than a few percent for any measurement.

2.3 Methods

We chose the core of the Pacific's Equatorial Undercurrent (EUC) at 140°W as our starting point and traced the particles backward in time until they intersected the local mixed-layer, crossed 55°S , or crossed 120°E south of Australia. We also allowed for the possibility of trajectories beginning in the Bering Sea, north of 65°N , or beginning in the Indian Ocean and flowing eastward through the Indonesian Throughflow, but neither of these paths was realized in any experiment. The choice of 140°W was somewhat arbitrary; our only criterion was to choose a longitude downstream of the Hawaii-to-Tahiti Shuttle Experiment data (Wyrтки and Kilonsky, 1984). For the annual

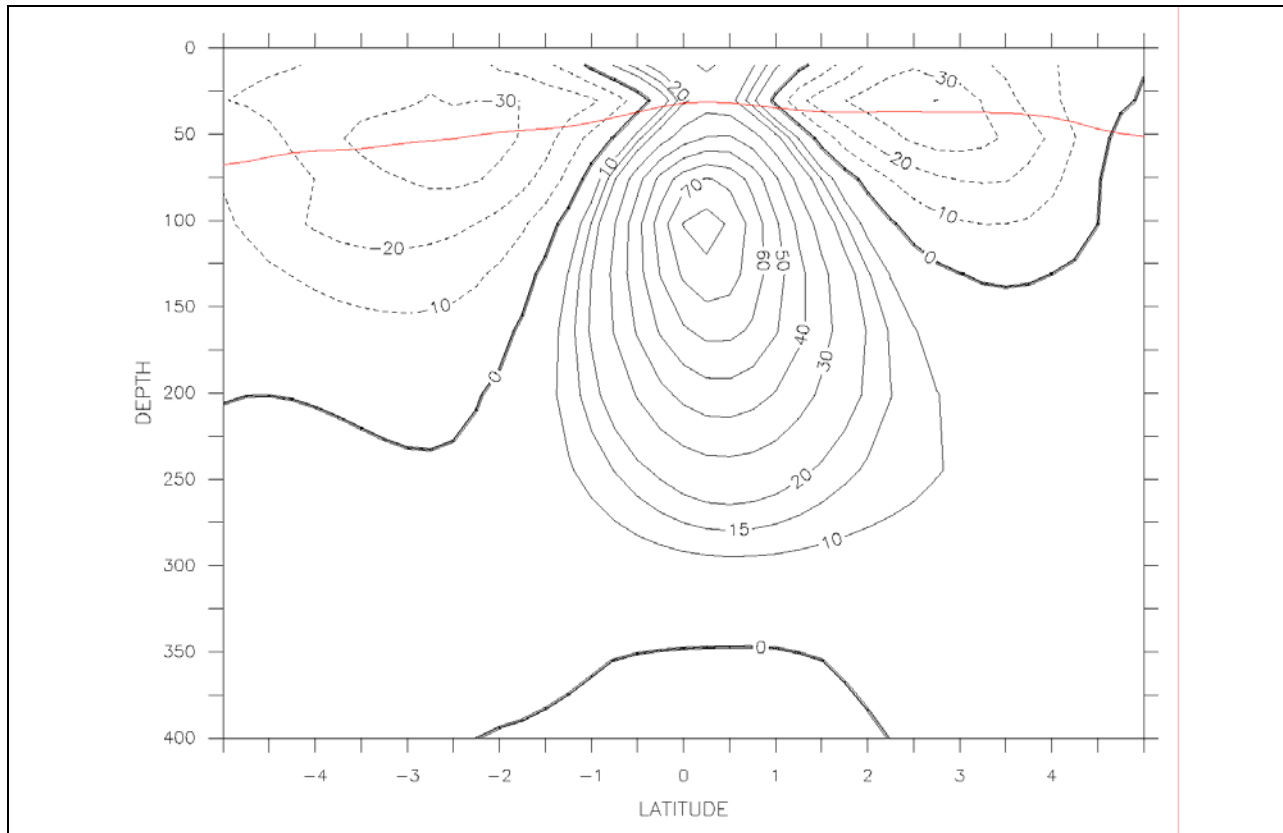


Figure 1: Equatorial Undercurrent speed (cm/s) at 140°W during the spring in OCCAM. The red line is the average springtime mixed layer depth.

runs, we used the annual mean EUC as our starting point, and the mixed-layer depths were determined from the annual-mean data. For the seasonal runs, we use each season's EUC and the deepest mixed-layer depth that occurs during the 3-month season. The core of the EUC is defined as those points between 3°S and 3°N where the zonal velocity is greater than 15 cm/s eastward (Fig. 1) and deeper than the mixed layer. These definitions for the EUC are fairly typical of other studies (Blanke and Raynaud, 1997, Rodgers et al., 2003) although ours is generally more restrictive by not including westward flowing particles and those moving too slowly.

The transport through each grid-box (the speed times the cross-sectional area) that meets this criterion is divided into roughly 2,500 parcels, which are seeded at regular intervals across the face of the grid-box. The EUC in OCCAM transports about 25 Sv ($25 \times 10^6 \text{ m}^3/\text{s}$) so there are approximately 10,000 trajectories calculated in the annual study and in the study in which we seeded once per season, while we follow ~

40,000 trajectories in the four-seedings-per-season run, and ~80,000 in the case with eight-seedings-per-season. The different number of calculated trajectories leads to different average sizes for each parcel: ~2500 m³/s (or 2.5 mSv, 1 milli-Sverdrup = 10³ m³/s) with 10,000 trajectories, ~620 m³/s with 40,000 trajectories and ~310 m³/s with 80,000 trajectories.

The mixed-layer depths (MLDs, Fig. 2) used in this study are the maximum MLD for each three-month season. Each month's MLD was defined as the depth over which the density is within 0.1 kg/m³ of the surface value. In comparison, Blanke and Raynaud (1997) define their EUC as those points at 150W with an eastward velocity, between 3.55°S and 3.55°N above 495m. Rodgers, et al. (2003) chose their starting criteria as all points along 151°W between 3°S and 3°N with an eastward velocity below the mixed layer and above 612 meters. Their mixed layer depth was defined as the point at which the density differed from the surface by 0.01 kg/m³, a definition that they note may be not well suited to the equatorial region as it leads to too shallow mixed layers in the tropics and a notable lack of ventilation sources between 10°S and 10°N. Also, their cut-off at 612m leads to the inclusion of parcels with a much greater density in EUC.

We emphasize that the trajectories in the model follow streamlines through the fluid, calculated solely from the velocity fields that are not necessarily coincident with isopycnals. The particles themselves have no inherent density; their location and age are calculated by the trajectory algorithm and the OCCAM density, temperature and salinity are mapped onto the particle. These are recorded at the starting and ending sections as well as several other intermediate sections.

We note that the relative statistics described here do not depend on the size of the particles: when we seeded the EUC with particles sizes smaller than 2500 m³/s, the ratio of southern to northern source waters and the fraction of particles intersecting the mixed layer differed by no more than a few percent. Although we tracked the particles backward in time, the following discussion will describe the simulation forward in time with the particles subducting out of the mixed-layer at the beginning, and their subsequent arrival at the EUC at the end.

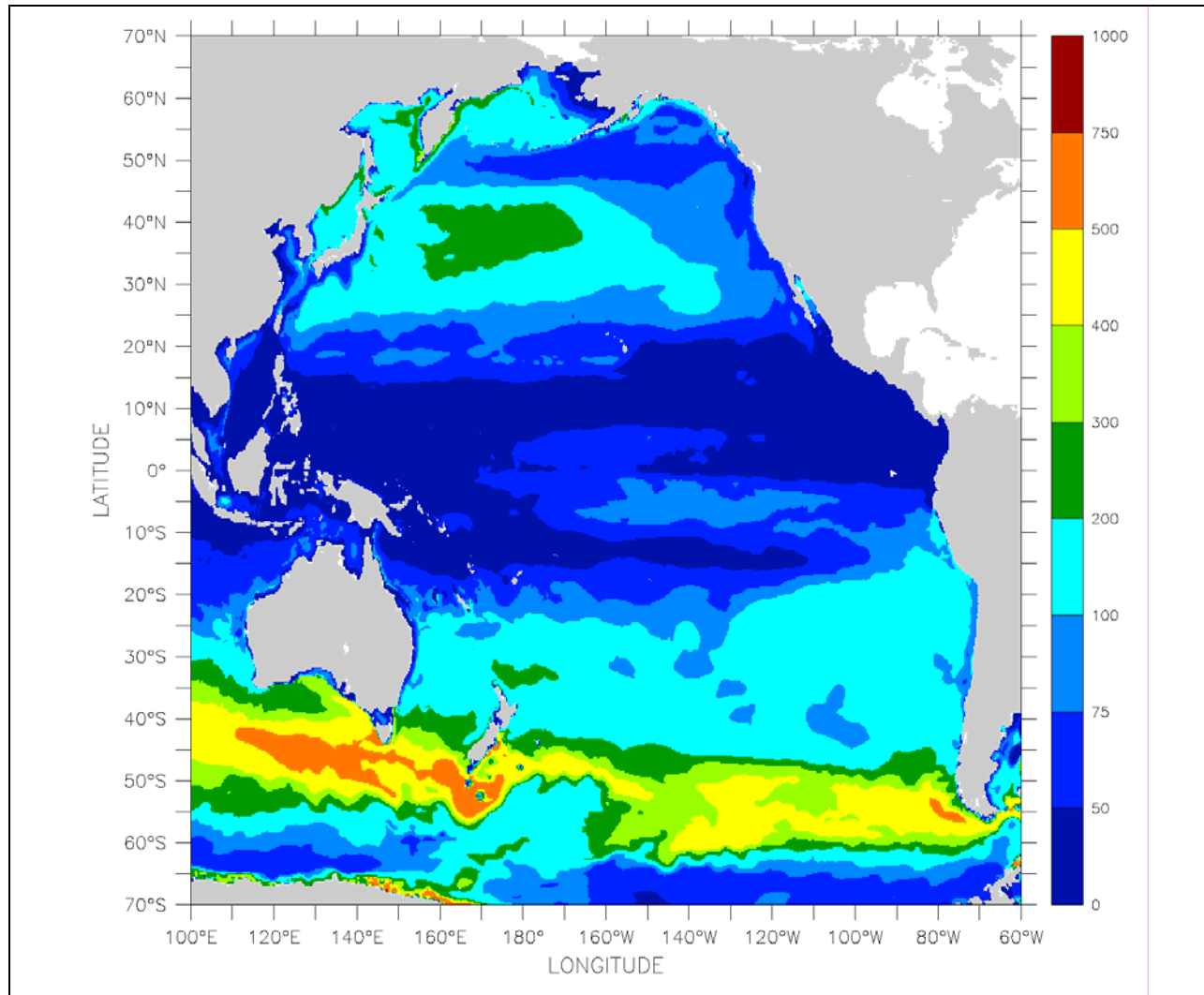


Figure 2: Maximum annual mixed layer depth (m) in OCCAM.

3. Sensitivity of the Trajectory Algorithm

We conducted several experiments with different velocity fields. These included annual mean velocities without the residual transport (Eulerian mean) and with the residual transport (Residual mean), seasonal mean velocities (Eulerian mean and Residual mean) and 5-day mean velocities. We also explored the effects of increasing the number of seedings per season to explore the sensitivity of the algorithm to both time of year and particle size.

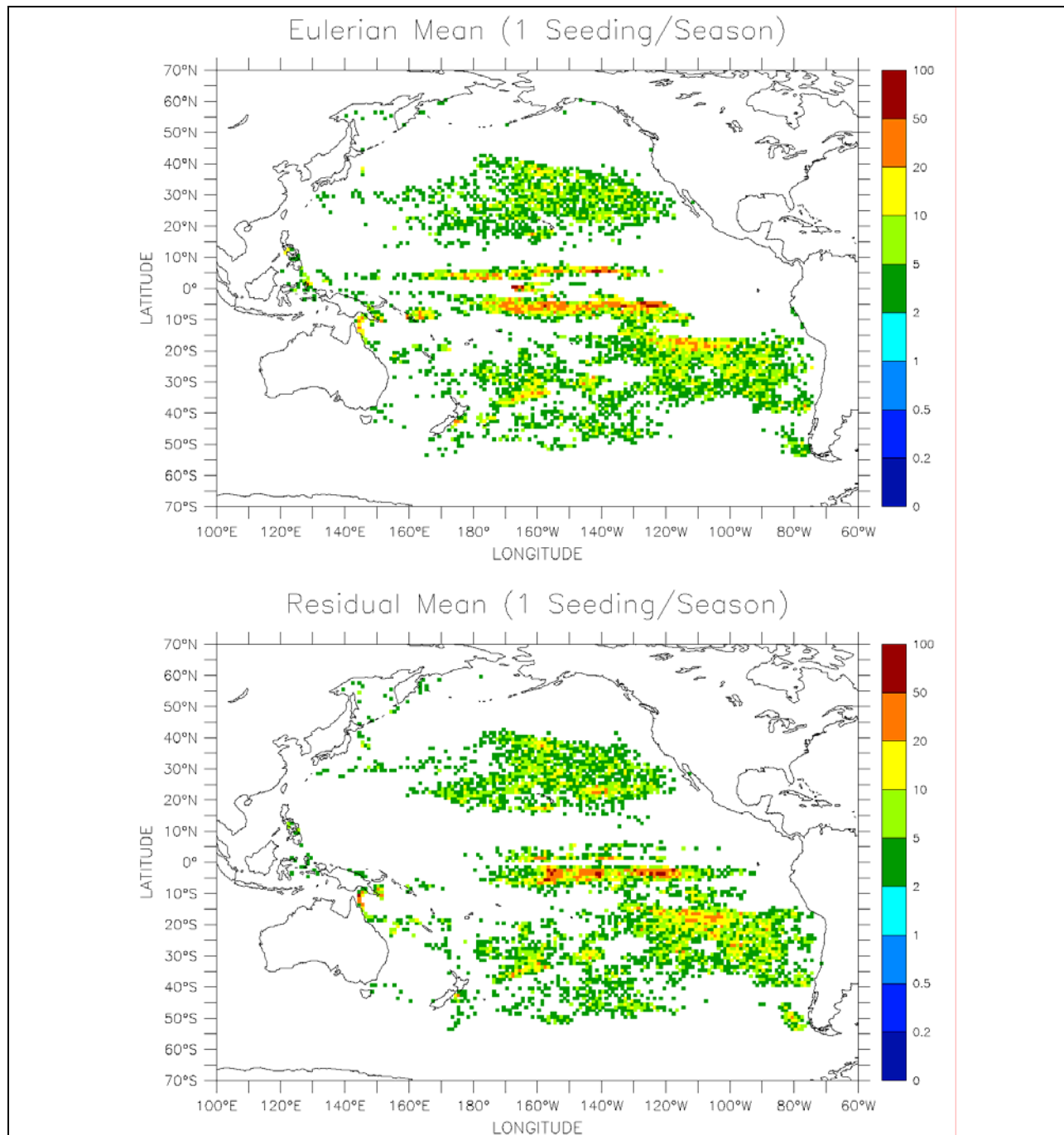


Figure 3: Volume (mSv) and initial location of water parcels ending in the EUC during the a) Eulerian Mean, and b) Residual mean seasonal experiments with one seeding per season giving an average particle size of $2500 \text{ m}^3/\text{s}$.

3.1 Eulerian mean vs. Residual mean

We first conducted experiments using two different velocity fields: the seasonal Eulerian mean velocities and the seasonal residual mean velocities. The strength of the

modeled EUC has a transport of 21-29 Sv in both cases. These agree well with the published estimates based on both current meters (32 Sv, Lukas & Firing, 1983; 23 Sv, 30 Sv, Wyrski and Kilonsky, 1984), and geostrophy (26 Sv, Lukas & Firing, 1983), especially considering that we have only included the core of the EUC. The locations where the backtracked trajectories intersect the mixed-layer were binned into $1^\circ \times 1^\circ$ boxes and their volumes were summed for each of the datasets. The experiments show that particles ending up in the EUC leave the mixed-layer in three main places (Figure 3): in zonal bands immediately to the north and south of the equator, with the southern band having a greater volume; broadly across the South Pacific with the larger part concentrated toward the eastern end of the sub-tropical gyre and the smaller part in the center of the gyre, northeast of New Zealand; and in the North Pacific toward the eastern end of the sub-tropical gyre.

The main effect of including the residual transports (Figure 3b) is that the zonal bands near the equator are less intense, closer to the equator and shifted to the east in the Residual mean runs compared to the Eulerian mean runs. Hazeleger, et al. (2001a), using the same OCCAM data, reported that the tropical cells in the Pacific disappear when the residual velocities are included in the calculation of the meridional overturning, consistent with the reduction of the number of trajectories leaving the equatorial bands. The elimination of the spurious diapycnal forces related to the tropical cells are a strong motivation for our inclusion of the residual velocities. Hazeleger, et al. (2003), reported that the Atlantic EUC, from the same OCCAM data, also showed the same eastward shift in the subduction sites when the residual velocities are used. Differences between that study and this one are largely due to the topographic differences between the Pacific and Atlantic basins. Also, the basin-wide meridional overturning circulation in the Atlantic causes a strong north-south asymmetry that is not present in the Pacific. Readers should refer to these studies for a more complete discussion of the differences between Eulerian mean and residual mean transports.

The spatial patterns and quantitative results presented here are consistent with previous studies. The three and 1/2 layer model used by Lu, et al. (1998) indicated about 2/3 of the EUC water originated south of the equator, the same ratio found here. Huang and Liu (1999) in the NCEP Ocean Model had less a greater percentage of

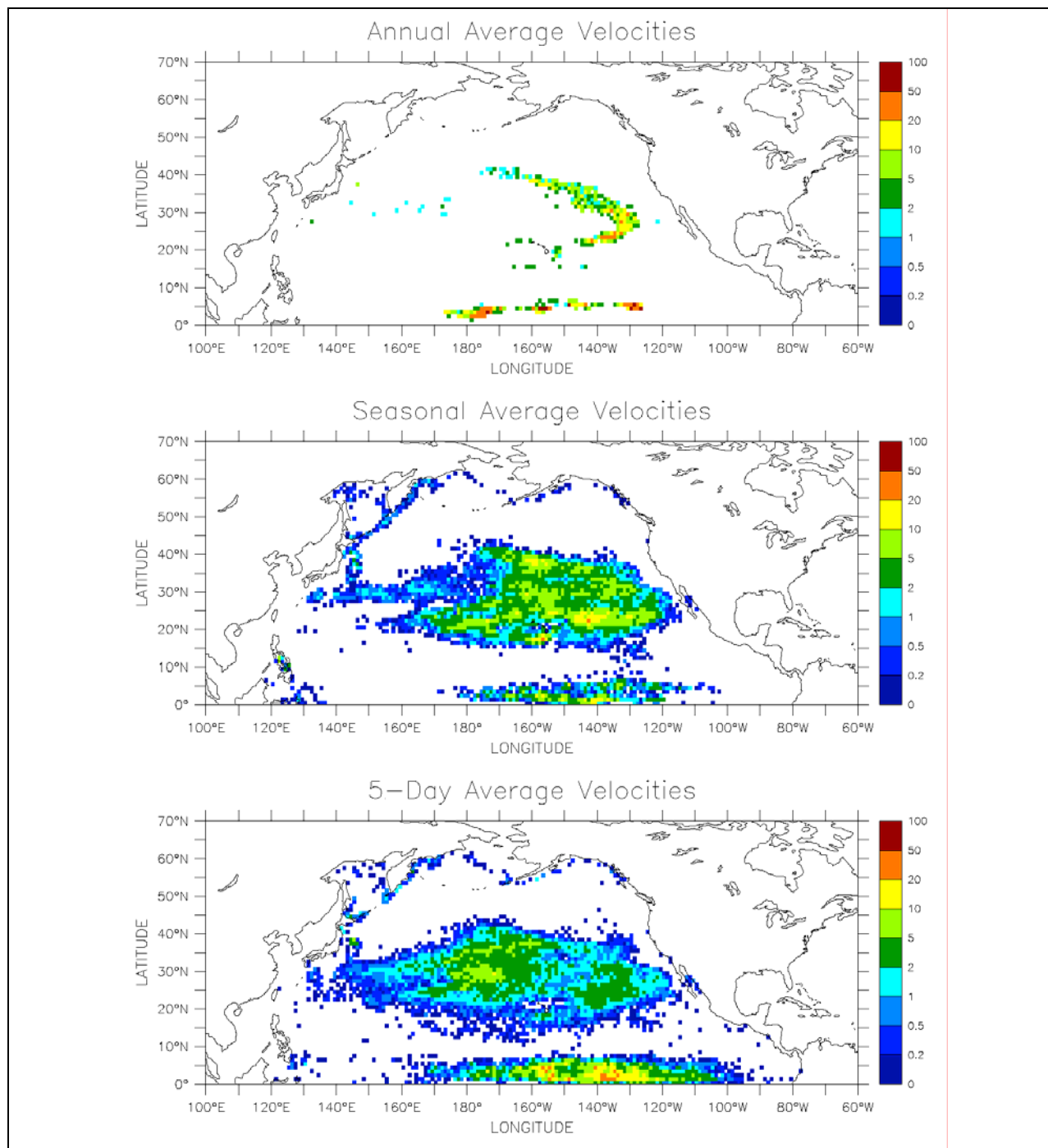


Figure 4: Volume (in mSv) and initial location of water parcels from the North Pacific ending in the EUC during a) the annual experiment, b) the seasonal experiment and c) the 5-day experiment. For each of these runs, we used the northern half of the EUC only and disallowed for trajectories crossing the Equator. For the annual and 5-day runs (Figs 4a, 4c), we used the first year of the last three years of data, while the seasonal run (Fig. 4b) includes all three years.

northern water in the EUC, but their model has no Indonesian Throughflow, which preferentially draws water from the north relative to the south.

3.2 Effects of Annual, Seasonal or 5-day averages

We next conducted several experiments in which we used three different sets of velocity fields: the annual average, the seasonal average, and the 5-day means of the velocity fields but with only one year of data. The trajectory algorithm requires that the entire velocity field for the year be held in active memory; using the 5-day means requires an eighteen-fold increase in the amount of computer memory necessary so these runs were carried out in a reduced domain covering only the North Pacific (north of 5°S). Each of these experiments uses the Eulerian mean velocity fields for the same model year. The use of only one year of data limits the proper construction of a residual mean transport, but as seen in Figure 3, the use of an Eulerian-mean instead of a residual mean does not affect the large-scale dispersion. Figure 4 shows the subduction sites for these three runs. For each of these runs, we used the northern half of the EUC and disallowed for trajectories crossing the Equator.

The differences between the annual experiment (Fig. 4a) and the other two are striking. The ventilation sites are much more diffuse in the seasonal and 5-day runs. These changes are due to the dispersion which comes from varying transport velocities instead of the uniform annual-mean transports. The inclusion of a varying mixed layer depth may also play a small role, in that particles are more likely to leave the mixed layer when the mixed layer shoals around them. In the annual mean experiment, the trajectories are carried away at a few well-delineated locations: along the eastern and northern edges of the subtropical gyre and in a band at 5°N. The dispersion of the trajectories between the seasonal (Fig. 4b) and 5-day (Fig. 4c) experiments has not changed significantly in comparison with the annual to seasonal mean differences. Differences between these two experiments include an increase and a spreading of the 5°N band in the 5-day run and a shift to the eastern end of the subtropical gyre in the seasonal run. Only 3.3 Sv are ventilated north of the equator in the annual experiment whereas the same 6.1 Sv are ventilated north of the equator in the other two runs. We

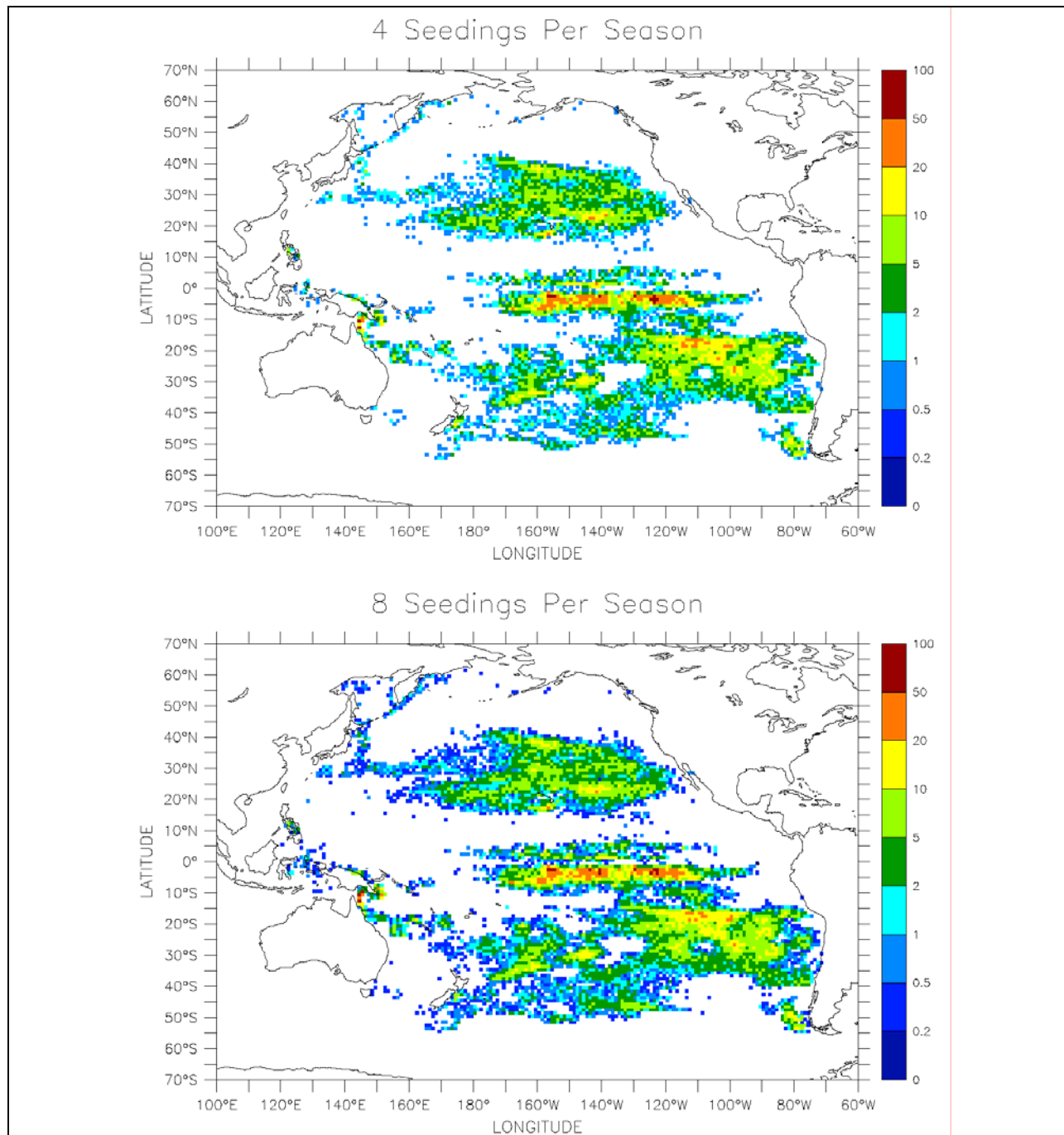


Figure 5: Volume (in mSv) and initial location of water parcels ending in the EUC during the Residual mean seasonal experiment with a) four separate seedings per season giving an average particle size of $620 \text{ m}^3/\text{s}$ and b) eight separate seedings per season giving an average particle size of $310 \text{ m}^3/\text{s}$.

must note, however, that there are interannual fluctuations that may lead to differences in the ventilation results. The similarity of Figures 4b and 4c, and the similar statistics of

sources and transports (they differ by no more than 10-15%), leads us to conclude that the use of seasonally averaged data does not significantly bias our results.

3.3 Effects of Seeding Frequency

The last sensitivity test we performed was on the frequency of particle seedings per season. The results from one seeding in the middle of each season were shown in Figure 3. The roughly 25 Sv EUC was divided into four, 2500 trajectory seedings giving a particle size of 2500 m³/s. We also divided the seeding of each season into four (Figure 5a) and eight (Figure 5b) parts. As noted above, four (eight) seeds per season is 16 (32) seeds per year giving an average particle size of 625 (310) m³/s. Increasing the number of trajectories leads to a greater dispersion in their sources, i.e. the infrequent sites shown in purple in Figure 5b are absent in Figures 3 and 5a, but the three figures are not qualitatively different. We want to reiterate that Drijfhout, et al. (2003) note that errors of up to 20% were found in simulations that use seasonal data sets and did not use some form of temporal interpolation. The rest of this study will focus on the results from the eight seedings per season, residual mean experiment.

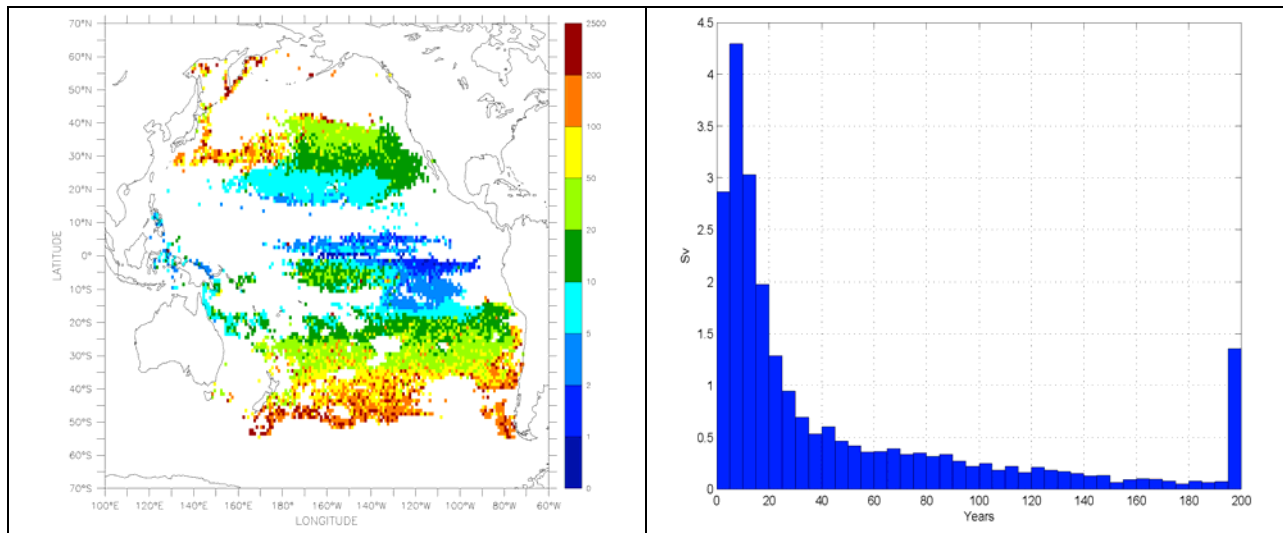


Figure 6: Time between subduction and the EUC in years a) plan view, and b) binned into 5-year windows. The last bin is the total volume that ventilates after year 195.

4. A Geographic Analysis

The Residual mean seasonal dataset has an annual mean EUC of 23.9 Sv at 140°W, varying from a low of 21 Sv in the winter to a high of 29 Sv in the spring (Fig. 1). Over 97% of the 76,869 trajectories (23.3 Sv) backtrack from the EUC into the mixed layer, and 2.5% (0.6 Sv) cross 55°S. (The remaining 13 trajectories begin at 120°E between Australia and 55°S.) Figure 5b shows that the ventilated portion (originating in the mixed layer) subducts primarily from the Southern Hemisphere (south of 13°S, 10.5 Sv) and the equatorial region (between 13°S and 10°N, 7.2 Sv) with a smaller portion from the Northern Hemisphere (north of 10°N, 5.5 Sv). Totals of 6.5 Sv and 0.7 Sv are ventilated in bands between 13°S and 0° and between 0° and 10°N, respectively. These are the South Equatorial Current (SEC) and North Equatorial Current (NEC) which are "the major upper ocean flows supplying the western boundary," (Fine, et al., 1994) and are therefore a conduit into the EUC. Of the 7.2 Sv ventilated in the equatorial region, 4.2 Sv or 58% never crosses beyond 10°N or 13°S before entering the EUC. The median time for equatorial trajectories between subduction and the EUC is 3.8 years for those that never leave the tropics, 15.1 years for those that do leave, and 4.7 years for all equatorial trajectories (Fig. 6).

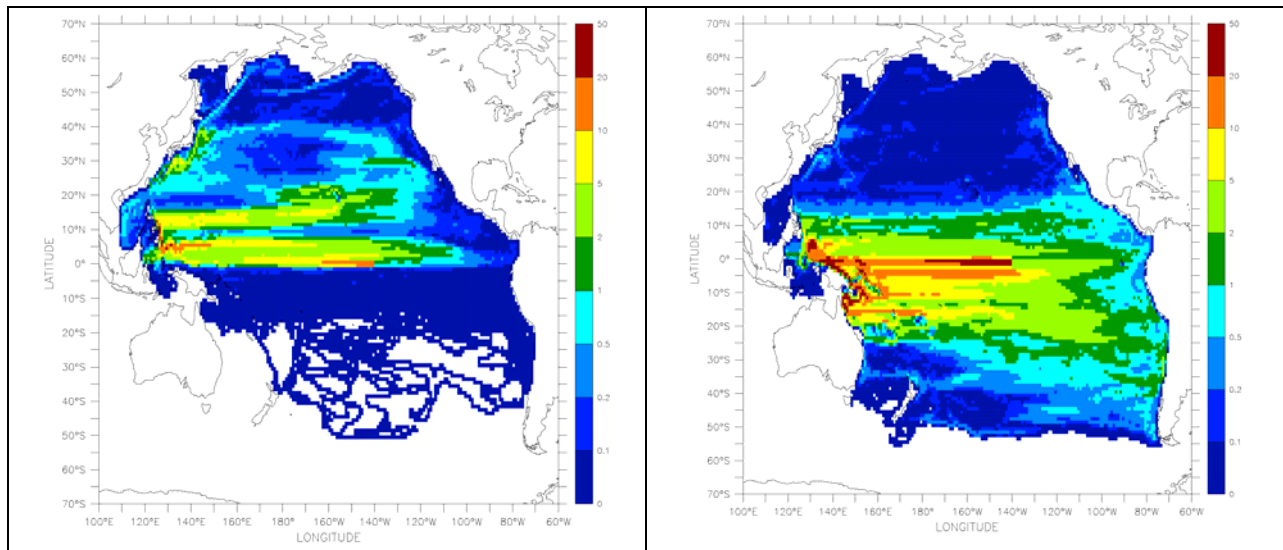


Figure 7: Positions occupied by the trajectories between subduction and the EUC (at any depth) for a) particles subducting north of the equator, and b) particles subducting south of the equator. Units are volume in 10^6 m^3 .

Summaries of the positions occupied by the trajectories are shown in Fig. 7. These summaries or "footprints" are calculated by integrating with depth and time the number of trajectories that pass through a given grid-cell. The footprints reveal where the particles have passed, regardless of depth or direction. For trajectories originating north of the equator (Fig. 7a), the major avenues are in the North Equatorial Current (NEC, the zonal band at 13°N), the Mindanao Current, the North Equatorial Countercurrent (NECC, the zonal band at 5°N, east of the Philippines), and the Equatorial Undercurrent. Moderate activity is also seen in the Kuroshio region and along the eastern edge of the gyre. Comparing northern trajectories to southern trajectories (Fig. 7b), the differences in cross-equatorial flow are striking. The fundamental differences between the Northern and Southern Pacific Oceans are due to the geometries of the coastlines, and to the presence of the Indonesian Throughflow (ITF). Water in the Mindanao Current will either flow through the ITF or turn eastward at 5°N to join the NECC. Only 1732 particles (out of 17,659) that leave the mixed layer north of the 10°N cross 5°S and their total transport is 0.04 Sv.

The southern hemisphere trajectories go everywhere: 4.4 Sv of South Pacific water cross 5°N and these particles recirculate an average of 4-5 times across this latitude before settling into the EUC. Many features of the equatorial current structure described by Fine, et al. (1994) are highlighted by the southern particles, including the New Guinea Coastal Current and the New Guinea Coastal Undercurrent (east of New Guinea), the several branches of the South Equatorial Current (zonal bands at 17°S and 4°S), the South Equatorial Countercurrent (at 10°S), and the Mindanao and Halmahera Eddies (at 5°N, 130°E and 1°N, 140°E, respectively). The bands of weaker activity at 10°N and 13°S motivated our choice of these latitudes to define our equatorial region.

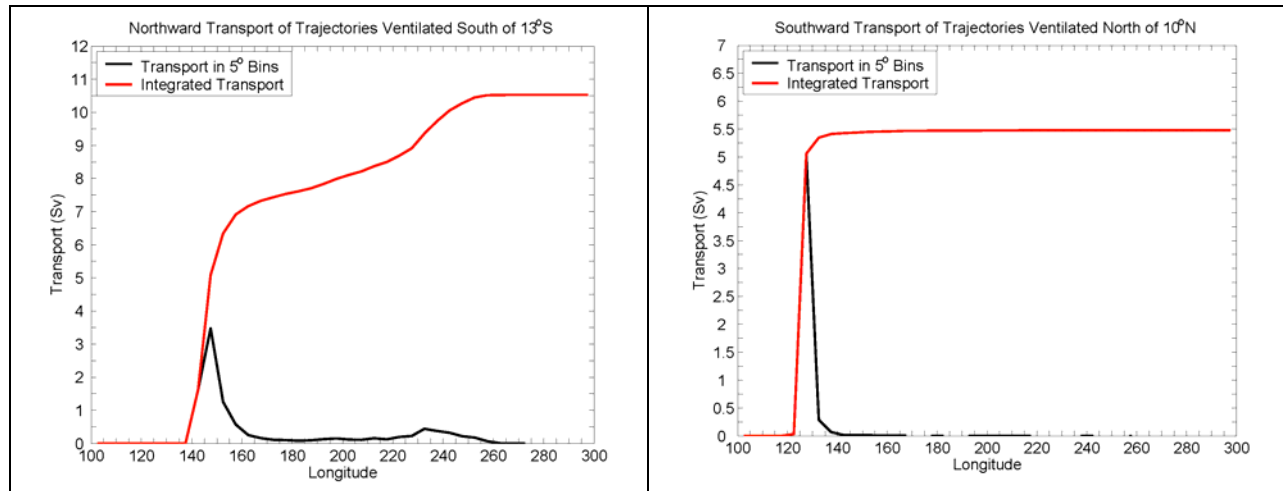


Figure 8: Transport across a) 13°S and b) 10°N binned by longitude. The black lines are the actual transport in each 5° longitude bin, and the red lines are the integrated transport (west to east).

In the South Pacific, 10.5 Sv are ventilated south of 13°S. These trajectories begin primarily in the eastern half of the subtropical gyre (Fig. 3). By definition, all of these trajectories end up in the EUC, so the longitude at which they cross 13°S headed northward for the last time is indicative of the path they take. Fig. 8a shows the transports of these trajectories at 13°S binned by longitude (black) and the integrated transport (red, beginning in the west). The particles that cross in the western boundary current as part of the SEC or the Great Barrier Reef Undercurrent between the northern tip of Australia and 160°E; these account for 6.9 Sv or 66% of the total. The separation between those trajectories taking an interior route (those that cross east of 160°W, totaling 3.6 Sv) and those in the western boundary is clear. The particles traveling through the western boundary have a median age of 14 years at the last crossing and a median age of 50 years when they enter the EUC (Fig. 6a). The interior particles have a median age of 10 years at 13°S, and 20 years at the EUC (Fig. 6a). Note again that trajectory ages and tracer ages are not identical. The large median age difference implies that particles following the western boundary route are more involved in recirculations and/or the zonal excursions seen in the footprints.

In the North Pacific, 5.5 Sv leave the mixed layer north of 10°N. Fig. 8b shows the longitude at which these trajectories cross 10°N southward for the last time. The western boundary is even more dominant than in the southern hemisphere with 5.1 Sv or 92% of the trajectories crossing between the Philippines and 130°E in the Mindanao

Current. These particles have taken a median transit time of 4.5 years to reach 10°N and then take an additional 9.3 years to reach the EUC (Fig. 6a).

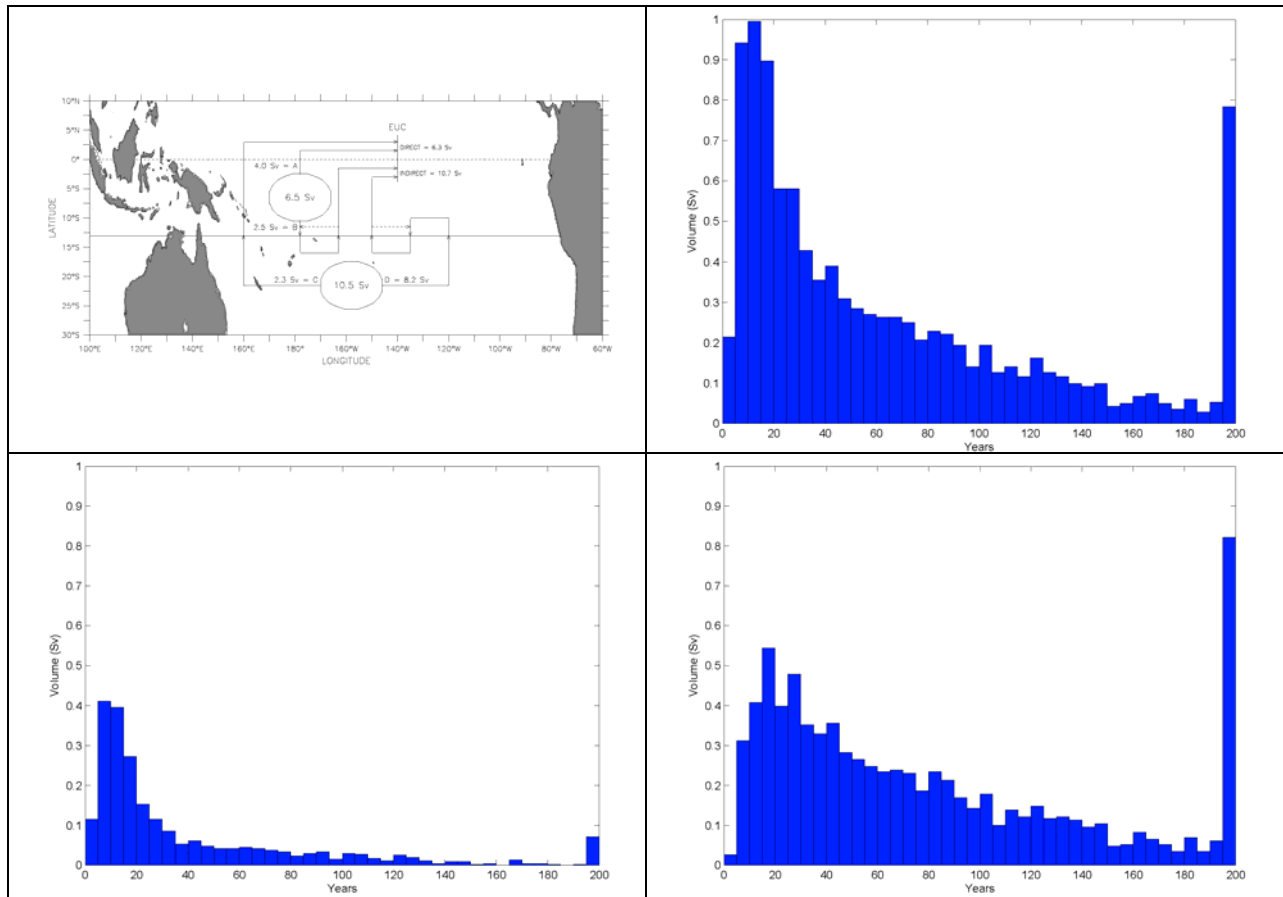


Figure 9: a) Cartoon of the possible paths for particles subducting south of the equator and ending in the EUC (17.0 Sv in total). Direct paths do not cross 13°S more than once, while indirect paths do. A and C are direct paths, B and D are indirect paths. The dashed lines represent possible additional recirculations. Please note that the positions of the pathways are not meant to indicate boundary current paths versus interior paths. b) Distribution of ventilation times for all trajectories ventilated south of 13°S, c) Distribution of ventilation times for path C trajectories, d) Distribution of ventilation times for path D trajectories.

Blanke and Raynaud (1997, their fig 9) show a much different census of the originating trajectories from both north and south of the equator. That study concludes that less than 25% of the water originating south of 15°S crosses that latitude in the boundary current, and over 50% of the water crosses between 130°W and 100°W. In the north, they have no EUC water moving southward in the Mindanao Current, and 80% of the northern-source EUC water crosses 15°N between 160°E and 120°W.

Recirculation, a difficult quantity and quality to measure in the real ocean, can be explored quite effectively with the trajectory algorithm. The large transports seen in Fig. 7 give a preliminary indication that many of the trajectories cross by the same point more than once on their journey from subduction to the EUC, and this is bolstered by the long times experienced by the particles as seen in Fig. 6. By summing the total transports at various intermediary sections, we can put a quantitative value on the total amounts of recirculation present in the velocity field. Fig. 9 is a cartoon of the possible paths by which a particle subducting south of the equator can travel to reach the EUC. If the particle subducts north of 13°S , the "direct" route has no southward or northward crossing of 13°S , and the "indirect" route must cross at least once in both directions. There are 6.5 Sv of EUC water ventilated between the equator and 13°S ; 4.0 Sv of this takes the direct route, consistent with the idea that the South Equatorial Current is fed into the Western Pacific "crossroads" and then returns eastward in the EUC. We can tell how many trajectories have ever crossed 160°E : that is, have been in the Western Pacific at some point in their journey. 94% of the particles are subducted east of 160°E and 77% of these cross 160°E at least once. Particles taking the direct route have a median travel time of 4.5 years until entering the EUC, whereas the indirect route particles have a median age of 16 years in the EUC.

For the trajectories originating south of 13°S , the median ventilation time is 43 years and the spectrum of ages is shown in Fig. 9b. This is somewhat misleading and our understanding of the circulation is substantially improved when we compare the direct and indirect paths. The direct route has precisely one northward crossing of 13°S , and the indirect route has at least one southward crossing. Of the total 10.5 Sv ventilated south of 13°S , 2.3 Sv cross 13°S only once, and the other 8.2 Sv make at least one recirculation, and average 3 southward crossings. As expected, the direct particles spend much less time between subduction and the EUC, 19 years versus 62 years for particles taking the indirect route. The spectrum of ventilation times shows that the direct path (Fig. 9c) has a steep drop after 20 years and a small tail of long-lived trajectories. The indirect trajectories (Fig. 9d) show a much more gradual decrease indicating the large amount of recirculation and points to the possibility of many transits into and out of the tropical band before the final entrainment into the EUC.

Name	Density Range (σ_θ)	Volume (10^6m^3)	% of the EUC	Median Age (years)
Tropical Water – north (TWN)	< 24.0	2.0	8.5	5.9
Tropical Water – south (TWS)	< 24.5	7.4	31.2	8.3
Eastern Subtropical Mode Water – north (ESTMWn)	24.0 < ... < 25.4	3.1	13.2	16.2
Eastern Subtropical Mode Water – south (ESTMWs)	24.5 < ... < 25.8	7.3	30.6	27.5
Central Subtropical Mode Water – north (CSTMWn)	25.4 < ... < 26.5	1.0	4.3	36.2
Central Subtropical Mode Water – south (CSTMWs)	25.8 < ... < 26.5	1.2	4.9	79.2
North Pacific Intermediate Water (NPIW)	> 26.5	0.02	0.1	106.4
Subantarctic Mode Water (SAMW)	> 26.5	1.1	4.7	129.7
Unventilated	> 27.0	0.6	2.6	1105.8

Table 1: Water masses which end up in the Pacific EUC in the OCCAM simulation

5. A Density Class Analysis

The previous section compared the trajectories based on their initial geographical location. We will now do an alternate analysis based on the initial density of the particles. Table 1 shows the initial density at which the ventilated trajectories leave the mixed layer. The density intervals were taken from the analysis of Fine, et al. (2001). Although these water masses are often defined by additional characteristics, such as potential vorticity, tracer content, etc., these intervals were chosen so that the model output from OCCAM could be compared directly to observations. We have defined North Pacific Intermediate Water (NPIW) as northern water with density greater than

26.5 and Subantarctic Mode Water (SAMW) as southern water with a density between 26.5 and 27.1. Fine, et al. (2001) also define Antarctic Intermediate Water (AAIW) with densities between 27.0 and 27.3, but there is almost none of that class represented north of 55°S in our experiment so we classify any ventilated southern water denser than 26.5 as SAMW.

The densities in the EUC are between 23.8 and 26.3, a reasonably wide spread, but as will be discussed later, the trajectories are well grouped in temperature/salinity (T-S) space. The EUC in the OPA model described by Rodgers, et al. (2003) has densities between 22.3 and 27.2, a significantly larger spread than seen in OCCAM, which is due to their starting criteria of all eastward-flowing water between 3°S and 3°N and above 612m. ESTMW is well delineated by the trajectory model, and accounts for about one half of each hemisphere's contribution to the EUC. CSTMW is also represented (1.2 Sv south, and 1.0 Sv north). The denser water masses (SAMW, NPIW) from each hemisphere make a small contribution to the EUC: only 1.1 Sv of SAMW from the south, and 0.02 Sv of NPIW make it to the EUC. There are, however, an additional 0.6 Sv that enter the domain across 55°S that never intersect the mixed layer before entering the EUC: 0.24 Sv are in the density range for AAIW (27.0 - 27.3) and these cross 55°S at depths between 500 and 1100m, while the rest likely represents Circumpolar Water.

		At Subduction										
		NH	TWN (2027)	ESTWN (3143)	CSTWN (1028)	NPIW (24)		SH	TWS (7436)	ESTWS (7303)	CSTWS (1162)	SAMW (1742)
In the EUC	TWN	-2018	0	1	0			TWS	-5977	105	4	7
	ESTWN	2017	-646	206	11			ESTWS	5968	-733	925	1703
	CSTWN	1	646	-207	13			CSTWS	9	628	-929	32
	NPIW	0	0	0	-24			SAMW	0	0	0	-1742

Table 2: The change in volume (in mSv) between subduction and the EUC as a function of water mass. The number in parenthesis is the initial volume (in mSv) of each water mass at subduction. Note that the unventilated water which enters the domain across 55°S is included in the water mass labeled as SAMW.

Since the denser water masses are formed at higher latitudes, it seems reasonable to look at the total meridional transport of all the trajectories at the most poleward sections of the model. The net equatorward flows of water with a density greater than 26.5 are 0.6 Sv at 20°N and 2.1 Sv at 30°S. Rodgers, et al. (2003), however, report that as much as 6-7 Sv originally denser than 26.2 ends up in the EUC (~20% of their total.)

The change in density from the starts of the trajectories (at subduction) to their ends (at the EUC) is summarized in Table 2. The lightest water masses (TWN and TWS) get denser. The subtropical water masses from the north remain roughly the same although 20% of the ESTWN gets reclassified into the denser CSTWN range and 20% of the CSTWN gets reclassified into the lighter ESTWN range. In the Southern Hemisphere, 90% eastern subtropical water (ESTWS) stays in the same density class from start to finish, whereas only 20% of CSTWS remains unchanged. The densest water masses initially (NPIW and SAWM) all get lighter by the time they reach the EUC, and 98% of the water from the ACC ends up in the ESTWS range.

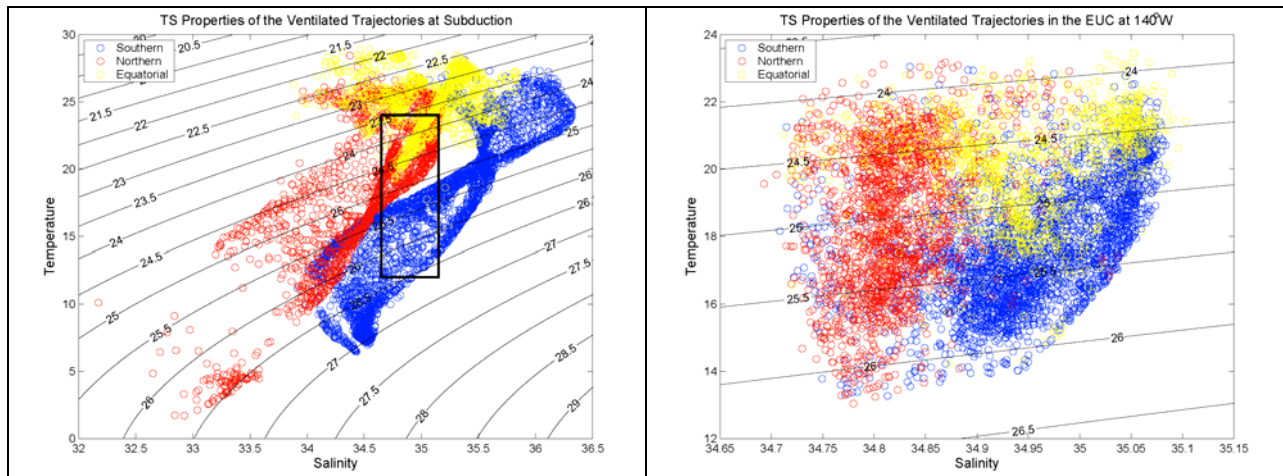


Figure 10: Temperature versus salinity characteristics for all of the ventilated trajectories a) at subduction, and b) in the EUC. The black box in a) matches the outer limits of b). Blue circles are trajectories originating in the South Pacific, red circles are trajectories originating in the North Pacific, and yellow circles are trajectories originating in the Equatorial Pacific.

6 A Hydrographic Analysis

Water masses are generally characterized by their temperature and salinity, so we present a hydrographic analysis of the water masses at the start, end and intermediate points along the trajectories. Fig. 10a shows the temperature versus salinity (T-S) properties of the ventilated trajectories at the point of subduction and Fig. 10b is an enlarged version of the EUC, color-coded by the location of ventilation. The EUC in OCCAM is a well-defined water mass with a small range in salinity and a larger range in temperature. As expected, the fresher particles in the EUC have mostly originated north of the Equator, the saltier ones have come from the south, and the equatorial particles are a bit warmer on average. Asking how and where the particles are transformed from their widely, disparate T-S properties at subduction to the tight grouping in the EUC (box in Fig. 10a) is equivalent to asking how and where the mixing processes occur.

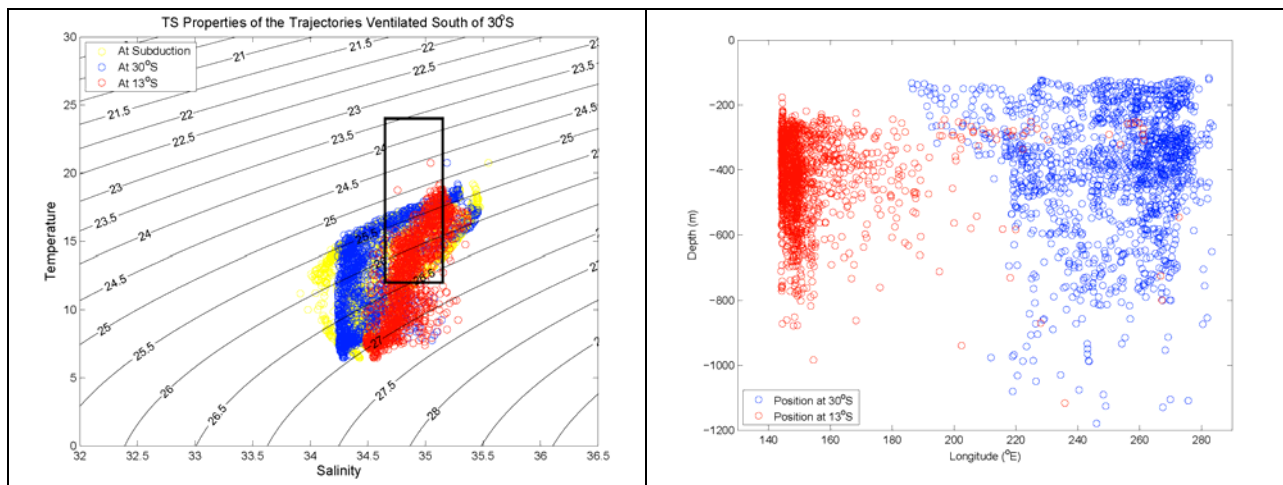


Figure 11: a) The temperature versus salinity characteristics of particles ventilated south of 30°S at subduction (yellow), crossing 30°S (blue), and crossing 13°S (red). b) The longitude versus depth of the same trajectories at 30°S (blue) and 13°S (red). The black box in a) matches the outer limits of Fig 10b.

A comparison of the T-S characteristics of the ventilated trajectories (3.5 Sv) beginning south of 30°S is presented in Fig. 11a. In the 23 years after being subducted

(yellow circles), these particles become slightly colder and fresher before they cross 30°S northward for the last time (blue circles, Fig. 11a,b), but there is still a reasonably wide spread in both temperature and salinity space. The particles are mostly in the northward flowing portion of the subtropical gyre as is seen in Fig. 11b. Crossing 13°S for the last time (red circles, Fig. 11a,b, 37 years later), these trajectories have been concentrated in T-S space, and again the range in salinity is reduced far more than the range in temperature. These trajectories take an additional 30 years to reach the EUC (a median transit time of 90 years from start to finish) where they are generally warmer and have a more uniform salinity (Fig. 10b).

7. Discussion

The sources of the Pacific Equatorial Undercurrent are explored using data from the OCCAM model and a volume-conserving trajectory algorithm. Backtracking the particles in the core of the EUC until they hit the seasonally varying mixed-layer reveals several critical facts relating to the sources of the EUC. The results of this study support the hypothesis that the ultimate source of the EUC water is extratropical: 20 of the 24Sv spend at least part of their lifetimes poleward of 5°S or 5°N. This tends to rebut the local recirculation hypothesis, although local recirculation between 5°S and 5°N is certainly present in the OCCAM simulation.

The trajectory algorithm can provide much information that is difficult or impossible to obtain from direct ocean measurements. The sensitivity of the algorithm to residual mean vs. Eulerian mean transports is shown to be consistent with previous studies. The sensitivity of the algorithm to annual vs. seasonal vs. 5-day velocity fields and to seeding frequency, is shown to be qualitative rather than quantitative if varying velocity fields are used. Using only the annual-mean velocity field leads to a substantial, and likely unrealistic, decrease in the dispersion of particles and trajectories. Quantitative estimates of the rates of recirculation, as well as determination of the main pathways and mixing time-scales are critical to both ocean tracer and climate studies.

Over 97% of the particles in the EUC started in the mixed-layer north of 55°S. The main subduction sites are south of 13°S in the eastern and central South Pacific

subtropical gyre, in the South and North Equatorial Currents, and north of 10°N in the eastern and central North Pacific subtropical gyre. The contribution from southern sources is more than double that of northern sources. There is quite a bit of recirculation across every meridional section as is indicated by the trajectory ages. The majority of the high-latitude trajectories enter the tropics for the last time in the equatorward flowing western boundary currents as described by Fine, et al. (1994). The T-S characteristics of the particles are well-mixed in these boundary currents but there is some evidence that much of the mixing (in the OCCAM simulation at least) occurs earlier in their path. There is in general more change in the T-S properties between subduction and the last crossing of a meridional section, than there is between that last crossing and the final EUC values. This is further proof that extratropical ventilation is more important than tropical recirculation is setting the properties of EUC water.

Johnson and McPhaden (1999, JM99 hereafter) report a net interior equatorward flow of 14 Sv at 8°S (east of 165°E) and 6 Sv at 8°N (east of 135°E). An analysis of the annually averaged transport in the OCCAM model versus density across these same sections is shown in Fig 12 [compare to JM99, Fig. 6]. The southern hemisphere transport (Fig. 12 a,c) is quantitatively and qualitatively similar to their results, but there is a significant disagreement north of the equator (Fig. 12b). While the overall shape of the transport is similar at 8°N, the model has a net northward flow across this section below 41m. The discrepancies between OCCAM and JM99 are not likely due to their assumption of a 900db level of no motion: we recalculated the OCCAM transports after subtracting the 900db flow and the results were quite similar. These differences might be due to the fact that the Ekman transport in OCCAM is felt below the 41m level or, conversely, that the mixed layer in JM99 is shallow: lighter water masses are included in their calculation but are excluded in ours. It is also possible that the OCCAM's western boundary current is too wide and our analysis is picking up some of the northward flow along the boundary, making our interior flow seem more northward than JM99.

JM99 and Fig. 12 include all water parcels crossing these latitudes and not just those that end up in the EUC. Our trajectory analysis, which only accounts for the flows into the EUC, shows a total interior flow of 3.6 Sv from the South Pacific (across 13°S

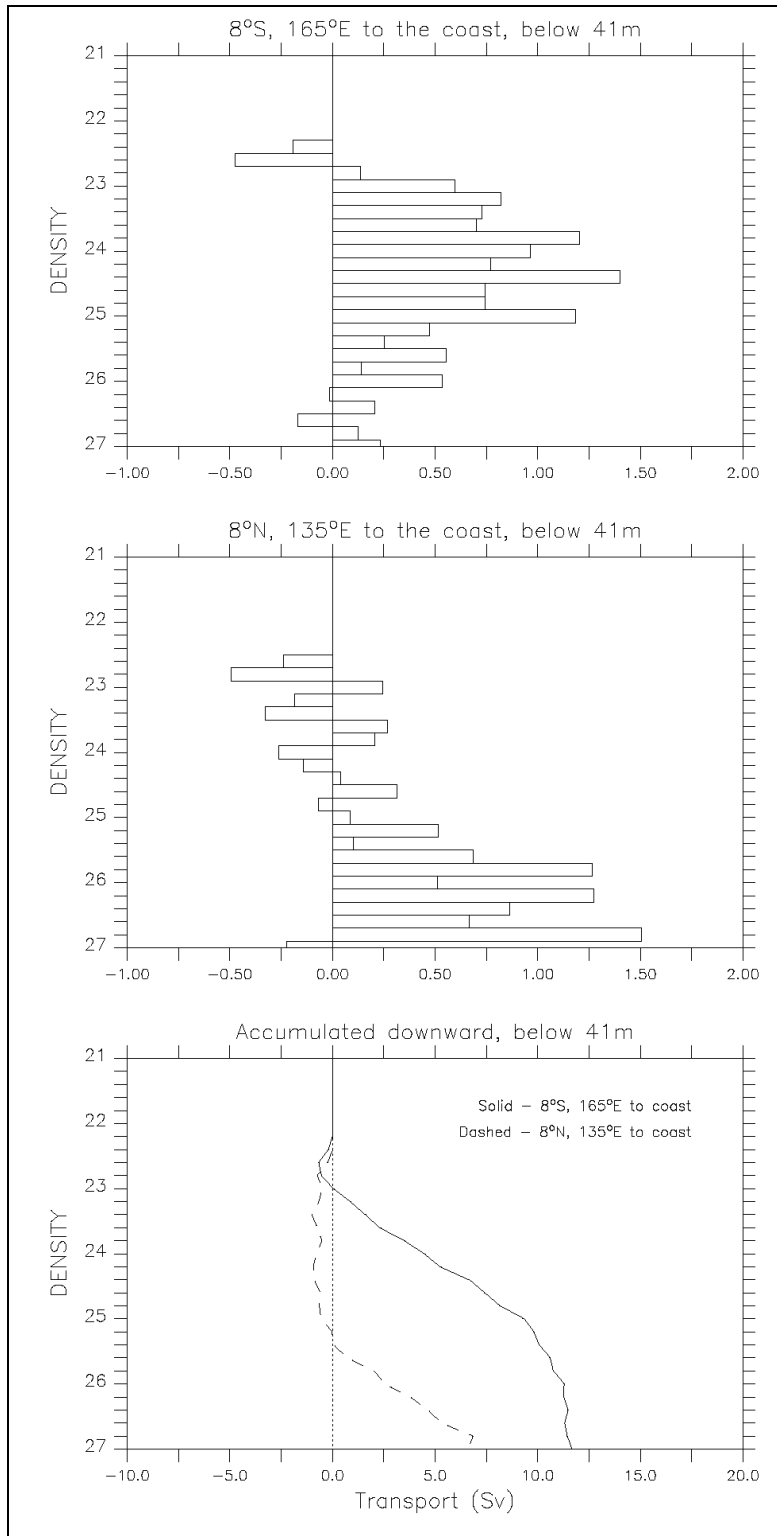


Figure 12: The net meridional transport binned in density every 0.2 kg/m³ from the South American coast to a) 165°E at 8°S, and b) 135°E at 8°N. Positive transport is northward. c) Transport at 8°S (solid) and 8°N (dashed) integrated downward. All units are Sv.

east of 165°E) and only 0.2 Sv from the North Pacific (across 10°N, east of 135°E). We should note that it is possible that there are interior paths from either hemisphere that join the EUC east of 140°W and are therefore not counted in our analysis. The strength of the EUC, however, gradually weakens toward the east, so additional interior contributions are likely to be small. Plots of the cumulative ventilation of the EUC against time and the total volume from each pentad (Figure 6b) show, in agreement with the CFC estimates of Fine, et al. (1994) and Fine, et al. (2001), that the median age of all ventilated particles at the EUC at 140°W is 19 years. About 70% had a transit time of less than 50 years, and 85% have an age of less than 100 years. Trajectories from the south take longer to arrive at the EUC than the trajectories from the north, due to the fact that North Pacific water is unlikely to cross the equator, whereas 79% of the trajectories starting south of 13°S cross 5°N.

The data for our analysis is from the seasonally averaged output of the OCCAM model and there are likely differences between our results and those that would be derived from a complete set of observations. The footprints (Fig. 7) and the transit times (Fig 6 and Figs 9b,c,d) are consistent with the observations derived from tracer studies. This study provides a more complete picture than is possible from observations, but it is limited by the quality of the model simulation. As models improve, the trajectory algorithm will become increasingly useful.

7. References

- Blanke, B., and S. Raynaud, 1997: Kinematics of the Pacific Equatorial Undercurrent: an Eulerian mean and Residual mean approach from GCM results. *J. Phys. Ocean.*, 27, 1038-1053.
- Cromwell, T., R.B. Montgomery, and E.D. Stroup, 1954: Equatorial undercurrent in the Pacific Ocean revealed by new methods. *Science*, 119, 648-649.
- de Vries, P., and K. Döös, 2001: Calculating Residual mean trajectories using time-dependent velocity fields. *J. Atmos. And Ocean. Tech.*, 18, 1092-1101.
- Döös, K., 1995: Interocean exchange of water masses. *J. Geophys. Res.*, 100, 13,499-13,514.

- Drijfhout, S.S., P. de Vries, K. Doos, and A.C. Coward, 2003: Impact of eddy-induced transport on the Lagrangian structure of the upper branch of the thermohaline circulation. *J. Phys. Ocean.*, 33, 2141-2155.
- Fine, R.A., R. Lukas, F.M. Bingham, M.J. Warner, and R.H. Gammon, 1994: The western equatorial Pacific: a water mass crossroads. *J. Geophys. Res.*, 99, 25,063-25,080.
- Fine, R.A., K.A. Maillet, K.F. Sullivan, and D. Willey, 2001: Circulation and ventilation flux of the Pacific Ocean. *J. Geophys. Res.*, 106, 22,159-22,178.
- Gibson, R., P. Kållberg, S. Uppala, A. Hernandez, A. Nomura, and E. Serrano, 1997: The ERA description, The ECMWF Re-Analysis Project Report Series, 1, ECMWF, Reading, UK.
- Gu, D., and S.G.H. Philander, 1997: Interdecadal climate fluctuations that depend on exchange between the tropics and extratropics. *Science*, 275, 805-807.
- Hazeleger, W., P. de Vries, and Y. Friocourt, 2003: Sources of the equatorial undercurrent in the Atlantic in a high-resolution ocean model. *J. Phys. Ocean.*
- Hazeleger, W. P. de Vries, and G.J. Van Oldenborgh, 2001a: Do tropical cells ventilate the Indo-Pacific equatorial thermocline? *Geophys. Res. Lett.*, 28, 1763-1766.
- Hazeleger, W., M. Visbeck, M. Cane, A. Karspeck, and N. Naik, 2001b: Decadal upper ocean temperature variability in the tropical Pacific. *J. Geophys. Res.*, 106, 8971-8988.
- Huang, B., and Z. Liu, 1999: Pacific subtropical-tropical thermocline water exchange in the National Centers for Environmental Prediction ocean model. *J. Geophys. Res.*, 104, 11,065–11,076.
- Johnson, G.C., and M.J. McPhaden, 1999: Interior pycnocline flow from the subtropical to the equatorial Pacific Ocean. *J. Phys. Ocean.*, 29, 3073-3089.
- Killworth, P.D., 1996: Time interpolation of forcing fields in ocean models. *J. Phys. Ocean.*, 26, 136-143.
- Lee, M.M., A.C. Coward, and A.J.G. Nurser, 2002: Spurious diapycnal mixing of the deep waters in an eddy-permitting global ocean model. *J. Phys. Ocean.* 32, 1522-1535.

- Levitus, S. and T.P. Boyer, 1994: World Ocean Atlas 1994. Vol. 4: Temperature: NOAA Atlas NESDIS 4, U.S. Govt. Printing Office, 117pp.
- Levitus, S., R. Burgett, and T.P. Boyer, 1994: World Ocean Atlas 1994. Vol. 4: Salinity: NOAA Atlas NESDIS 3, U.S. Govt. Printing Office, 99pp.
- Lu, P., J.P. McCreary, and B.A. Klinger, 1998: Meridional circulation cells and the source waters of the Pacific Equatorial Undercurrent, *J. Phys. Ocean.* 28, 62-84.
- Lukas, R., and E. Firing, 1984: The geostrophic balance of the Pacific Equatorial Undercurrent. *Deep-Sea Res.*, 31, 61-66.
- McDougall, T.J., 1998: Three-dimensional residual mean theory. *Ocean Modelling and Parameterization*, E.P. Chassignet and J. Veron, Eds, Kluwer, 269-302.
- McIntosh, P.C., and T.J. McDougall, 1996: Isopycnal averaging and residual mean circulation, *J. Phys. Ocean.*, 26, 1655-1660.
- Pacanowski, R.C., and S.G.H. Philander, 1981: Parameterization of vertical mixing in numerical models of tropical oceans. *J. Phys. Ocean.*, 11, 1443-1451.
- Rodgers, K., B. Blanke, G. Madec, O. Aumont, P. Caias, and J.C. Dutay, 2002: Extratropical sources of equatorial Pacific upwelling in an OGCM. (submitted).
- Saunders, P.M., A.C. Coward, and B.A. de Cuevas, 1999: Circulation of the Pacific Ocean seen in a global ocean model: Ocean Circulation and Climate Advanced Modelling project (OCCAM), *J. Geophys. Res.*, 104, 18,281-18,299.
- Schneider, N., S. Venzke, A.J. Miller, D.W. Pierce, T. Barnett, C. Deser, and M. Latif, 1999: Pacific thermocline bridge revisited, *Geophys. Res. Lett.*, 26, 1329-1332.
- Tsuchiya, M., 1981: The origin of the Pacific Equatorial 13°C Water, *J. Phys. Ocean.*, 11, 794-912.
- Tsuchiya, M., R. Lukas, R.A. Fine, E. Firing, and E. Lindstrom, 1989: Source waters of the Pacific Equatorial Undercurrent, *Prog. Ocean.*, 23, 101-147.
- Webb, D.J., A.C. Coward, B.A. de Cuevas, and C.S. Gwilliam, 1997: A multiprocessor ocean general circulation model using message passing. *J. Atmos. and Ocean Tech.*, 14, 175-183.
- Webb, D.J., B.A. de Cuevas, and A.C. Coward, 1998: The first main run of the OCCAM global ocean model. Internal report, Southampton Oceanography Center, 44pp.

[Available from Southampton Oceanography Center, Empress Dock,
Southampton SO14 3ZH, United Kingdom.]

Wyrski, K., and B. Kilonsky, 1984: Mean water and current structure during the Hawaii-to-Tahiti Shuttle Experiment. *J. Phys. Ocean.*, 14, 242-254.

Zhang, R.H., L.M. Rothstein, and A.J. Busalacchi, 1998: Origin of upper-ocean warming and El Niño change on decadal time scales in the tropical Pacific Ocean. *Nature*, 391, 879-882.